Journal of Colloid and Interface Science 363 (2011) 175–181

Contents lists available at ScienceDirect

Journal of Colloid and Interface Science

www.elsevier.com/locate/jcis

Gold nanoparticles modified ZnO nanorods with improved photocatalytic activity

Lanlan Sun, Dongxu Zhao *, Zhiming Song, Chongxin Shan, Zhenzhong Zhang, Binghui Li, Dezhen Shen

Key Laboratory of Excited State Processes, Chinese Academy of Sciences, Changchun Institute of Optics, Fine Mechanics and Physics, 16 East Nan-Hu Road, Open Economic Zone, Changchun 130033, People's Republic of China

ARTICLE INFO

Article history:
Received 19 May 2011
Accepted 4 July 2011
Available online 21 July 2011

Keywords:
Gold
Nanoparticle
Zinc oxide
Nanorod
Photocatalytic

ABSTRACT

Well-aligned ZnO nanorods (NRs) were grown on indium–tin-oxide (ITO) slide by the hydrothermal method and used as templates for preparing ZnO/Au composite nanoarrays. The optical and morphological properties of ZnO/Au composites under various $HAuCl_4$ concentrations were explored via UV–vis absorption spectroscopy, photoluminescence (PL) and scanning electron microscopy (SEM). The density and size of gold nanoparticles (Au NPs) on ZnO NRs can be controlled by adjusting the concentration of $HAuCl_4$. The optimal ZnO/Au composites display complete photocatalytic degradation of methyl blue (MB) within 60 min, which is superior to that with pure ZnO NRs prepared by the same method. The reason of better photocatalytic performance is that Au NPs act as electron traps and it prevents the rapid recombination of electrons and holes, resulting in the improvement of photocatalytic efficiency. The photocatalytic performance of ZnO/Au composites is mainly controlled by the density of Au NPs formed on ZnO NRs. The application in rapid photodegradation of MB shows the potential of ZnO/Au composite as a convenient catalyst for the environmental purification of organic pollutants.

1. Introduction

The degradation of toxic and hazardous molecules from wastewater has attracted much attention. The photocatalytic reaction has been a promising method to transform the pollutants into nontoxic molecules and eliminate the environmental pollution. Among semiconductors, TiO_2 and ZnO as photocatalysts exhibit good performances due to their high photosensitivity and non-toxicity [1,2]. However, a main limitation of high photocatalytic efficiency in semiconductors is the quick recombination of charge carriers, because the electron–hole pairs generated in semiconductor by optical irradiation can be easily recombined due to the direct band gap [3]. Therefore, the photoinduced charge separation in semiconductors is crucial in improving photocatalytic activity. In order to overcome this limitation, loading of noble metallic nanoparticles (NPs) on semiconductor seems to be a potential strategy, because the metals can store electrons within them and act as sinks for photoinduced charge carriers, promoting interfacial charge-transfer processes [4–7]. And with this aim, combination of semiconductor and noble metal has been the subject of many researches.

Several groups have reported that the photocatalytic activities were enhanced when noble metallic NPs (such as Au, Ag, and Pt) were deposited on semiconductor nanorods (NRs) [8,9]. For example, Zeng et al. reported that Pt/ZnO porous nanocages exhibited excellent photocatalytic performance, which can be attributed to the abundant nanoscale Schottky contacts in the Pt/ZnO interfaces [8]. Usually, there were three fundamental strategies to fabricate semiconductor oxide-noble metal hybrid nanostructures. The first strategy was selective growth of metals onto the tips and surfaces of semiconductor nanostructures [10]; the second strategy was growth of semiconductors on metal NPs seeds [11,12]; and the third strategy was diffusion of metallic NPs into semiconductors [13]. Among the noble metallic NPs, Au NPs have greater potential to decorate ZnO NRs for improving the photocatalytic activity. Au NPs are relatively stable, catalytically active, water-soluble, optically sensitive and with universal biocompatibility. The unique optical properties have enabled extensive applications of Au NPs as surface-enhanced Raman scattering (SERS) active substrates [14,15]. Joshi et al. have investigated the preparation of Au NPs decorated ZnO nanowires and their application for CO sensing at room temperature, and an enhancement in gas sensing response by Au decoration on ZnO nanowires was observed [16]. Many progress have been achieved in this research field, but much room remains for developing a stable and active Au NPs-modified ZnO NRs (Au/ZnO) photocatalysts. And up to now, there is no report about the influence of Au NPs density on the photocatalytic performance of ZnO NRs.

In this work, we provided a facile method to construct ZnO/Au hybrid nanostructures by directly growing Au NPs on aligned ZnO NRs arrays without adding any linking molecules. The optical properties of the created hybrid nanostructures were characterized, and the experimental results indicate that the optical properties are influenced by the density of Au NPs. In addition, ZnO/Au hybrid was used as photocatalyst for photodegradation of methyl blue

* Corresponding author. Fax: +86 431 4627031.
E-mail address: dxzhao2000@yahoo.com.cn (D. Zhao).

0021-9797/$ - see front matter © 2011 Elsevier Inc. All rights reserved.
doi:10.1016/j.jcis.2011.07.005

(MB) dye. It is demonstrated that the catalytic activity firstly increases and then decreases as Au NPs amount increases. In addition, it is found that ZnO/Au NRs with optimal density (9 per NR) display the highest photocatalytic efficiency to MB. The ZnO/Au hybrid nanostructures provide a new way to enhance the photocatalytic efficiency by designing desirable hybrid nanocomposites.

2. Materials and methods

2.1. Materials

Zinc acetate dihydrate ($ZnAc_2{\cdot}2H_2O$) was purchased from Aldrich. Hexamethylene tetramine (HMT) and methyl blue (MB) were purchased from Exciton Chemical, Co., Inc. (United States). Zinc nitride ($Zn(NO_3)_2$), chloroauric acid trihydrate ($HAuCl_4{\cdot}3H_2O$), sodium hydroxide (NaOH), ethanol, and methanol were all A.R. grade in purity and bought from Beijing chemical reagent factory (Beijing, China). All of these chemicals were used as received. The water used throughout this work was ultrapure water (18.2 MΩ cm) produced by a Milli-Q system.

2.2. Preparation of ZnO NRs

ZnO NRs arrays were prepared according to the method of Lee et al. with some modifications [17]. Briefly, cleaned indium–tin-oxide (ITO) slide was wet with a droplet of 0.02 M $ZnAc_2{\cdot}2H_2O$ in ethanol, rinsed with ethanol after 25 s, and blown dry with N_2. This wetting procedure was repeated three more times, and the sample was heated to 350 °C in air for 20 min in order to obtain ZnO seeds layers. The ITO slide with ZnO seeds was then vertically immersed into a growth solution (0.025 M $Zn(NO_3)_2$, 0.025 M HMT) and heated to 92.5 °C for 1 h. It should be indicated that the surface area of ITO slides is about 1 cm^2.

2.3. Preparation of ZnO/Au hybrid nanostructures

ZnO/Au hybrid nanostructures were prepared by a hydrothermal method. A volume of 20 mL of $HAuCl_4$ aqueous solution with different concentration (0.15–0.75 mM, initial concentrations) and 1 mL methanol were mixed under stirring. The pH of the solution was adjusted to 7–8 using 1 M NaOH solution under stirring. ITO slide with ZnO NRs was then suspended vertically in aforesaid solution and stirred slowly for 1 h. Then the solution was transferred to a stainless steel autoclave, and ITO slide with ZnO NRs arrays was immersed vertically followed by hydrothermal reaction at 120 °C for 1 h. After cooling to room temperature with cooling water, samples were washed with ultrapure water and dried under N_2.

2.4. Instruments

The morphology and structure properties of samples were investigated by field-emission scanning electron microscopy (FESEM, Hitachi S-4800), energy-dispersive X-ray spectroscopy (EDS, GENE SIS 2000 XMS 60S, EDAX, Inc.) XRD data were collected on a D/max-RA X-ray spectrometer (Rigaku). UV–vis absorption spectra were collected in solid using a Cary 500 UV–vis-NIR spectrophotometer. Photoluminescence (PL) measurements were performed using a He–Cd laser line of 325 nm as the excitation source.

3. Results and discussion

3.1. Characterizations of ZnO NRs arrays

Fig. 1a shows the typical SEM image of ZnO NRs on ITO substrate, which shows that ZnO NRs are well aligned and uniform over a large scale. The density of ZnO NRs was estimated to be about 16 per μm^2. The diameter of ZnO NRs was in the range of 100–150 nm. XRD pattern was shown in Fig. 1b, in which the diffraction peaks from ITO were marked by a symbol ▼. The 2θ diffraction peaks at 34.8°, 45.7°, 63.2° corresponded to (0 0 2), (1 0 2) and (1 0 3) ZnO wurtzite structure facets, respectively. The XRD pattern of ZnO NRs on glass substrate was also shown in Fig. 1b, in which the 2θ diffraction peaks at 34.8°, 36.4°, 63.1° corresponded to (0 0 2), (1 0 1) and (1 0 3) ZnO wurtzite structure facets, respectively. The strong peak of (0 0 2) confirms that the ZnO NRs have a preferred [0 0 0 1] growth direction. The photoluminescence (PL) spectra were characterized by a He–Cd laser with an excitation wavelength of 325 nm at room temperature. Fig. 1c shows the PL spectrum of as-prepared ZnO NRs on ITO. The UV peak at around 379 nm associated with its exciton emission at room temperature was observed. A broad band related to defects ranged from 500 to 700 nm in the visible light was also observed. The broad band may be caused by discrepancies, such as O vacancies, Zn vacancies, Zn interstitials, O interstitials, donor acceptor pairs, and surface state [18,19]. Such an energy absorption edge shows a potential of improving photocatalytic activity [20].

3.2. Morphological characterizations of ZnO/Au composite nanoarrays

Fig. 2a shows the morphology of the ZnO/Au NRs arrays prepared under proper $HAuCl_4$ concentration (Sample A). When the concentration of $HAuCl_4$ was 0.6 mM, Au NPs were coated on the surfaces of ZnO NRs. The average diameter of Au NPs was approximately 20 nm. The density of Au NPs on the surface of ZnO NRs was estimated to be approximately 9 per NR, which was obtained by counting and averaging the numbers of Au NPs on 100 NRs. To prove whether Au NPs decorate the hexangular surface or the whole surface including the lateral faces, a control experiment was carried out. Firstly, low-density ZnO NRs were fabricated by decreasing the wetting times to only once. Then ZnO/Au hybrid nanostructures were prepared by the same procedure, except that the concentration of $HAuCl_4$ was decreased to 0.3 mM. It can be seen from SEM image that Au NPs decorated the whole surface including the hexangular surface and lateral faces (data not shown). Here, low-density ZnO NRs were used because it is difficult to observe the lateral faces for high-density ZnO NRs. Lee et al. reported that as more Au NPs attached onto the surfaces of ZnO nanoneedles, most of the tips of the nanoneedles bended and attracted to form bundles [21]. But as-prepared ZnO/Au NRs showed higher rigidity and did not bend and form bundles. The diameter and length play an important role in keeping the rigidity, as the NRs with larger diameter and smaller length would be more rigid than that with smaller diameter and larger length as cores. Energy dispersive X-ray spectroscopy (EDS) (Fig. 2b) confirms that the samples consist primarily of Zn and Au.

To examine the effect of $HAuCl_4$ concentration on the growth of ZnO/Au NRs, a different concentration of $HAuCl_4$ was used. Fig. 3a–d shows SEM images of ZnO/Au NRs arrays prepared when the initial concentration of $HAuCl_4$ is 0.75, 0.45, 0.3, 0.15 mM, respectively (Samples B1–4). When the concentration of $HAuCl_4$ was as high as 0.75 mM, a very dense Au NPs film were coated on the surfaces of ZnO NRs (Fig. 3a). It is revealed that ZnO NRs were coated fully by the Au NPs with a size approximately 20 nm. When the concentration of $HAuCl_4$ was 0.45 mM, Au NPs (approximately 10 nm) were attached uniformly on the surface of ZnO NRs (Fig. 3b). As the concentration of $HAuCl_4$ was decreased, lower density of Au NPs were located on the surface of ZnO NRs (Fig. 3c). When the concentration of $HAuCl_4$ was 0.15 mM, almost no Au NPs were formed on the surface of ZnO NRs (Fig. 3d). The results shown in Figs. 2 and 3 suggest that the density of Au NPs on the

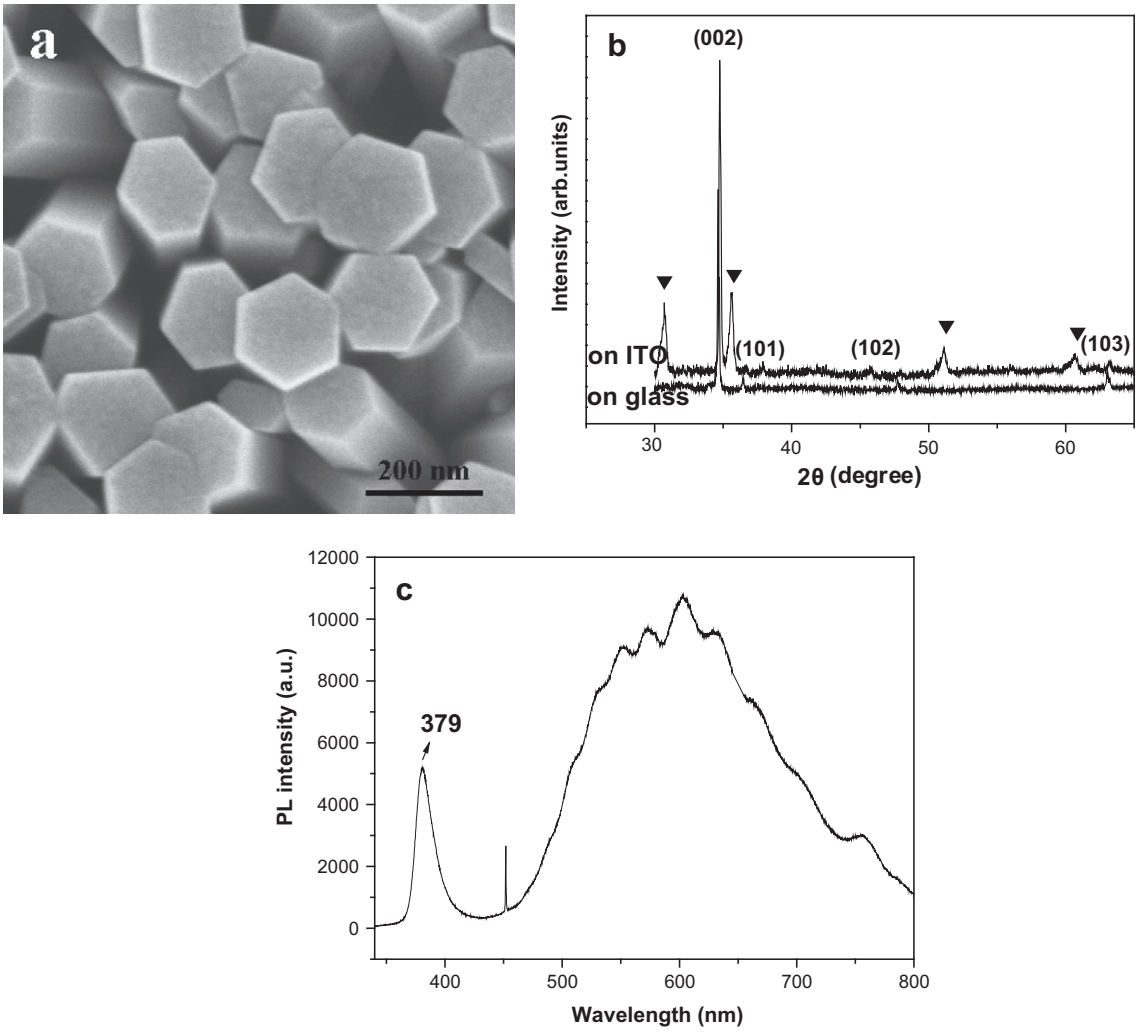

Fig. 1. (a) SEM image, (b) XRD pattern and (c) RTPL spectrum of ZnO nanorods on ITO substrate; XRD phase peaks from ITO are marked by a ▼ symbol; XRD pattern of ZnO nanorods on glass substrate is also shown in (b).

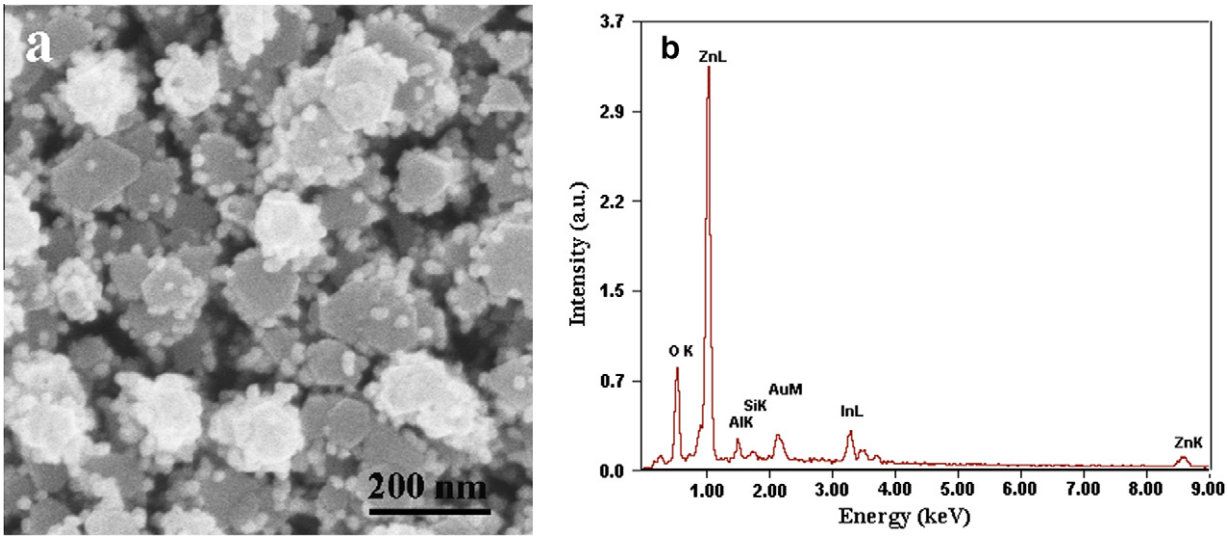

Fig. 2. (a) SEM image and (b) EDS spectrum of ZnO/Au hybrid nanocomposites (the initial concentration of $HAuCl_4$ is 0.6 mM), which corresponds to Sample A.

surface of ZnO NRs could be easily tuned by altering the concentration of $HAuCl_4$.

To further investigate the formation of ZnO/Au NRs, Au NPs without ZnO NRs core were synthesized directly on ITO substrate.

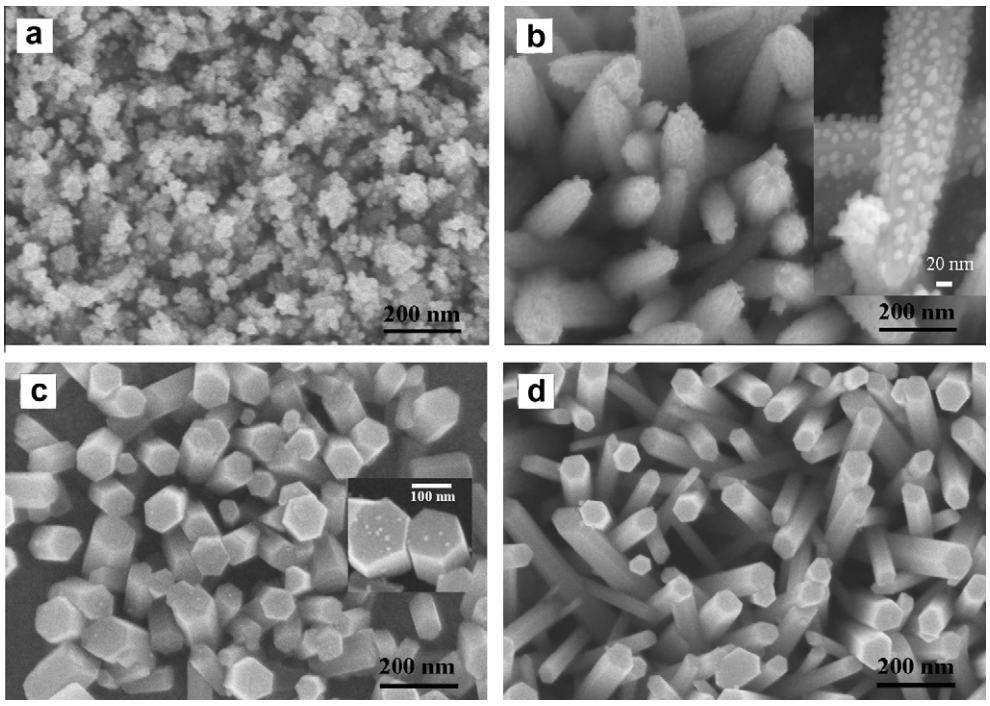

Fig. 3. SEM images of ZnO/Au hybrid nanocomposites with different concentrations of $HAuCl_4$: (a) 0.75, (b) 0.45, (c) 0.3, and (d) 0.15 mM, which correspond to Samples B1–4. The inset in images (b and c) are corresponding high-magnification SEM images.

Fig. 4a shows the SEM image of as-synthesized Au NPs on ITO substrate. Unlike the small-size Au NPs in Figs. 2 and 3, larger Au NPs were formed, and a statistical analysis reveals that the mean diameter of particles was 37.2 ± 0.5 nm (Fig. 4b). Fig. 4c shows the UV–vis absorption spectrum of pure Au NPs on ITO substrate. Two absorption peaks can be found in this spectrum. One broad peak around 561 nm indicates the formation of gold NPs, and another broad peak at about 437 nm is due to the localized surface plasmon resonance (LSPR) of indium–tin-oxide (ITO). It should be noted that the absorption spectrum of Au NPs on ITO has a red shift in comparison with the surface plasmon band (about 520 nm) of Au NPs in colloids (shown in Fig. 4c). The red-shift of the surface plasmon absorption is attributed to the strong interfacial coupling between Au NPs, which is in accordance with SEM result shown in Fig. 3a.

3.3. The optical properties of ZnO/Au NRs

Fig. 5 shows the UV–vis absorption spectra of ZnO/Au NRs grown on ITO substrate. The absorption peak between 300 and 400 nm was attributed to the absorption of ZnO in the UV light region. An obvious character is that there was a broad band appeared at 500–600 nm and there was also a long tail extended to the long wavelength scale. It is suggested that Au NPs were formed in the samples, and the broad band can be attributed to the coupling of the plasmon absorbance of the closely spaced Au NPs. In comparison with pure Au NPs (37.2 ± 0.5 nm) on ITO substrate (shown in Fig. 4c), the characteristic Au plasmon band in ZnO/Au composite was distinctly blue-shifted from 561 to 518 nm (Sample A), and to 522 nm (Sample B2). The blue-shift of surface plasmon absorption is attributed to the size decreasing of Au NPs (Sample A, 20 nm and B2, 10 nm). But for Sample B1, the characteristic Au plasmon band was obviously broadened and red-shifted from 561 nm to 573 nm, which demonstrates that Au NPs had a slight aggregation on the surface of ZnO NRs.

Fig. 6 shows the room temperature PL spectra of ZnO NRs and ZnO/Au nanocomposites. The PL spectra were composed of two emission bands in the UV and visible ranges, which were similar to that of the pure ZnO NRs. The UV emission band centered at 379 nm originates from the excitonic recombination, which occurs due to recombination between the electrons in conduction band and the holes in a valence band. The visible emission band between 500 and 700 nm is due to the recombination of electrons in a deep defect level or a shallow surface defect level with holes in a valence band [22]. ZnO/Au NRs exhibited weaker UV and visible emission than that of pure ZnO NRs. The ratios of the UV and visible emission band heights increased from ~0.5 to ~5.0, and UV/visible ratio reached the highest value (~5.0) for Sample A. It has been shown in Fig. 4c that as-synthesized pure Au NPs had a strong absorption in the visible range, which may contribute to the quenching of the visible emission of ZnO NRs when Au NPs were introduced. Another explanation for visible quenching is the surface passivation of ZnO NRs caused by Au NPs growing in oxygen vacancies or defects on the surface of ZnO NRs. The surface passivation makes energy potential high enough to prevent surface states trapping the electrons or holes photogenerated, which blocks the pathway to form luminescence centers.

3.4. Photocatalytic activities of ZnO/Au NRs

The photocatalytic capability of as-synthesized ZnO/Au NRs was investigated on degradation of the organic dye of methyl blue (MB). The concentration (C) of MB solution was characterized by the maximum absorption peak at about 662 nm (λ_{max}) by UV–vis spectroscopy. The photocatalytic process was demonstrated by the variation of λ_{max}. If no UV light irradiation was used, the concentration of MB was unchanged even after 90 min, indicating that less than UV-detectable amount of MB was decomposed (data not shown). Fig. 7 shows the evolution of degradation processes with the assistance of ZnO/Au NRs catalysts (Sample A). A continuous decrease of MB absorption by increasing irradiation time could be observed. Moreover, there was no new peak appeared during the process, which indicates the degradation of possible intermediate

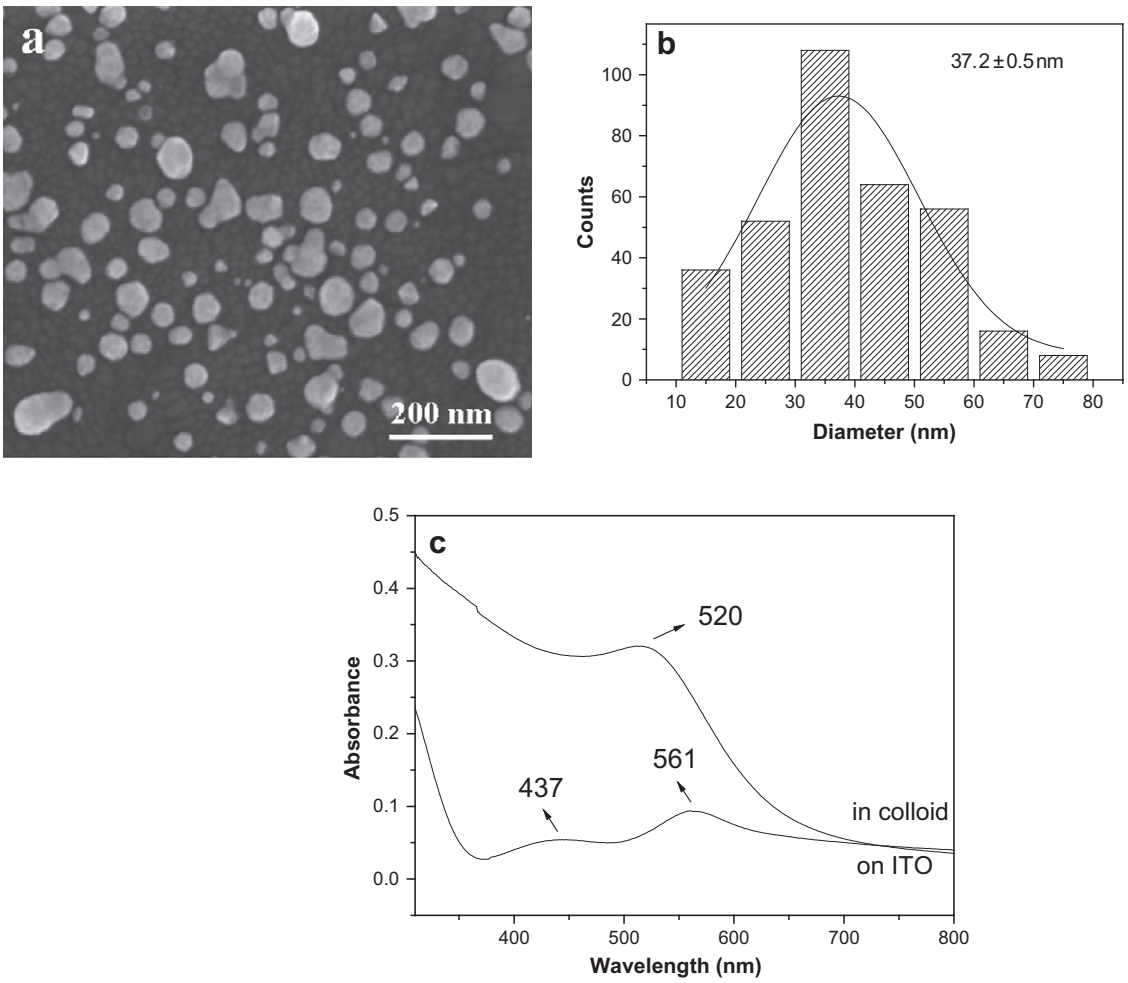

Fig. 4. (a) SEM image, (b) corresponding diameter distribution histogram, and (c) UV–vis absorption spectrum of gold nanoparticles gown on ITO substrate; UV–vis absorption spectrum of gold colloid is also shown in figure c.

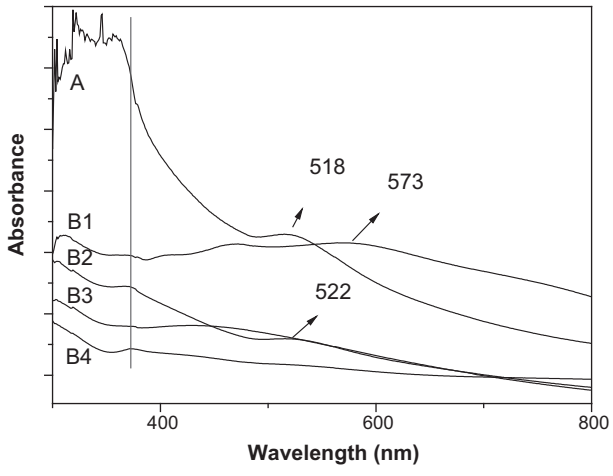

Fig. 5. UV–vis absorption spectra of Samples A and B1–4.

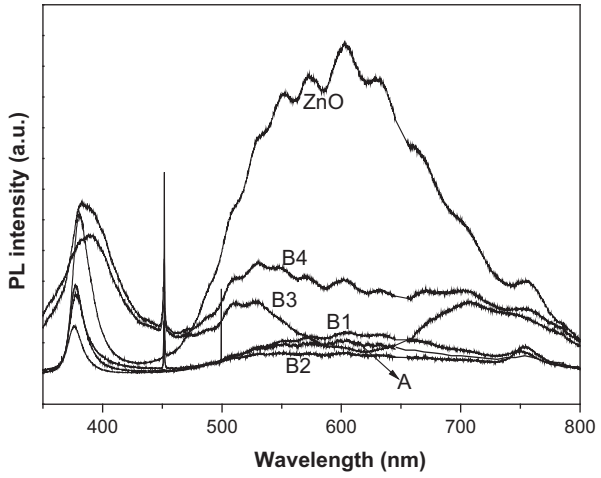

Fig. 6. The RTPL spectra of pure ZnO nanorods and ZnO/Au nanocomposites (Samples A, B1–4).

products. And no characteristic absorption of MB completes can be seen after irradiation for 60 min, which indicates that the photocatalytic degradation of MB may complete within 60 min.

Fig. 8 shows the photocatalytic degradation of MB (initial concentration: 5×10^{-5} M) as a function of irradiation time with different catalysts. The degradation of MB can be described by Langmuir–Hinshelwood mechanism: $\ln(C/C_0) = kt$. C_0 is initial concentration of MB, C is the concentration of MB depending on irradiation time, and k is reaction rate constant. An increase in $-\ln(C/C_0)$ corresponds to a decrease in the degradation of MB occurred under irradiation. It is indicated that Sample A shows the best capability and decomposed about 100% of MB after 60 min,

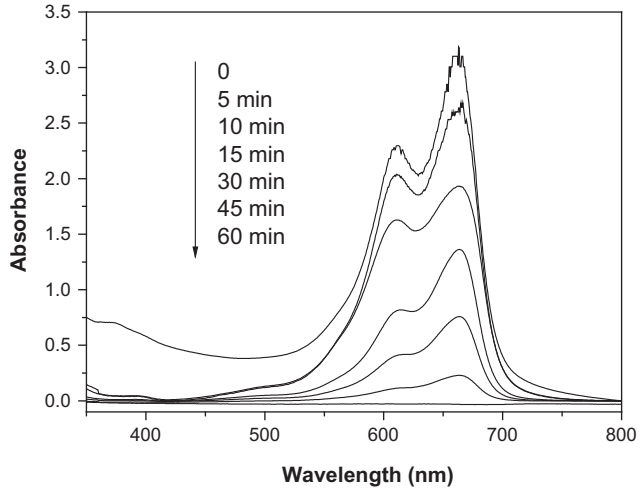

Fig. 7. UV–vis absorption changes of MB (5×10^{-5} M) in the presence of ZnO/Au NRs (Sample A) in different UV irradiation time.

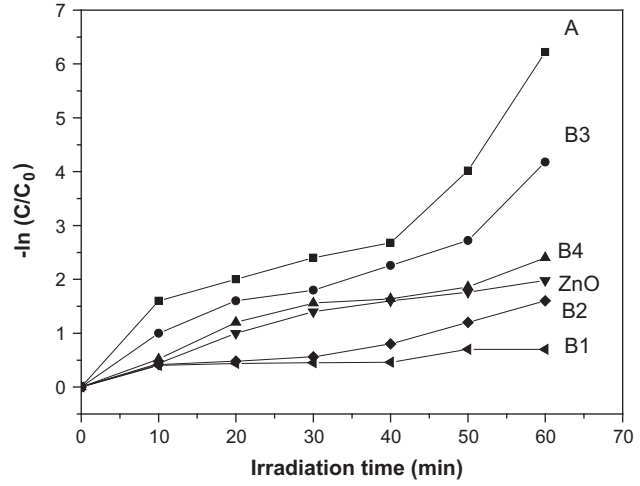

Fig. 8. Photocatalytic activities of Samples A and B1–4 upon irradiation time in the presence of fixed initial concentration of MB (5×10^{-5} M).

while Sample B1 shows the poorest photocatalytic performances. Compared with SEM results, it can be observed that the photocatalytic activity increased (from B4, B3 to A) and then declined (From B2 to B1) with an increase in the amount of Au NPs. As a control experiment, pure ZnO NRs were used as catalysts for degradation of MB, which was also shown in Fig. 8. It reveals that pure ZnO NRs show poorer capability than Samples A, B3, B4, but show better capability than Samples B1, B2.

It is very important to explain why different ZnO/Au NRs display different photocatalytic activities. The mechanism of photocatalytic process of ZnO/Au NRs is proposed as follows. The ZnO NRs act as electron and hole sources. The electron–hole pairs (EHP) of ZnO are generated by UV excitation. The electrons on the conduction band (CB) relax to the defect level and then react with electron acceptors O_2 to form superoxide anion radicals $O_2^{\cdot-}$, and the holes in valence band (VB) react with water to form hydroxyl radicals $OH^{\cdot-}$ [23]. The photocatalytic activity is mainly associated with the $O_2^{\cdot-}$ amount [24]. But the electrons for the formation of $O_2^{\cdot-}$ can be lost by EHP recombination. Au NPs act as sinks of photogenerated electrons and induce a shift of the Fermi level toward more negative potentials [4]. The ZnO/Au interface can transfer electrons from ZnO to Au by a charge equilibration process and lower EHP recombination to enhance the photocatalytic activity. In addition, For ZnO n-type semiconductor, the work function ($\varphi_s \approx 4.3$ eV) is less than that of the noble metals ($\varphi_{m\mathrm{Au}} \approx 5.1$ eV, $\varphi_{m\mathrm{Pt}} \approx 5.65$ eV), and thus, a Schottky barrier will form at the junction, resulting in an inhibition of the electron injection from the semiconductor conduction band into the metal and facilitating the electron capture.

Table 1
Photocatalytic activities of ZnO/Au hybrid with various Au NPs density and size.

Sample	Au NPs density (per NR)	Au NPs size (nm)	Photocatalytic activities order
A	9	20.0	1 (strongest)
B1	50	20.0	4
B2	500	10.0	5 (weakest)
B3	2–3	9.5	2
B4	1	9.1	3

The photocatalytic activity orders of ZnO/Au hybrid with various Au NPs density and size were summarized in Table 1. From Table 1, it reveals that the photocatalytic activities of the ZnO nanorods are indeed affected by the density of Au NPs, and the photocatalytic activities order of ZnO/Au hybrids is: B2 < B1 < B4 < B3 < A. SEM images indicate that Au NPs density and size increased from B4, B3, to A, and their photocatalytic activities increased correspondingly. The higher efficiency of ZnO/Au (B4, B3, to A) can be explained by two reasons: one is that Au NPs act as electron traps to impede electron/hole recombination [25], the other one is that Fermi level equilibration between Au NPs and ZnO may decrease the band gap of ZnO and hence diminishes the rapid electron/hole recombination [26,7]. From SEM images, the surfaces of B1 and B2 were almost fully covered with Au NPs, which showed lower photocatalytic activities. The main reason for the poor performance is that the covered Au NPs reduced the surface contact area between MB and ZnO. We suggest that the density of Au NPs on ZnO NRs is a main factor for the enhancement of photocatalytic activity. It can be seen from Figs. 2 and 3 that the density of Au NPs increased with the increase in $HAuCl_4$ concentration. It has been reported that 2% Au content is optimum to achieve the highest efficiency of photodegradation for TiO_2 NPs [27,28]. On observing the SEM images of ZnO/Au NRs and the corresponding photocatalytic activities, we found that the ZnO/Au NRs with a proper Au NPs density (9 per NR, Sample A) displayed greater photocatalytic activity than other samples with different Au NPs density. Higher Au NPs density could be an obstacle to photocatalytic performance. The reason is that when the density of Au NPs is below the optimum density, Au NPs act as electron–hole separation centers, which improves the photocatalytic activity of ZnO. When the density of Au NPs is higher than the optimum density, Au NPs act as electron–hole recombination center, thus decreasing the photocatalytic activity of ZnO. Similar result has been observed by Yoon et al. that the hole-capture is increased when a large number of Au NPs were attached onto TiO_2 surface, which reduces the efficiency of charge separation [2].

The size and density of Au NPs on ZnO NRs are synchronously changed with the change of $HAuCl_4$ concentration. Therefore in this work, it is difficult to synthesize Au NPs with same density and different size with the method, so we cannot study the effect of Au NPs size on ZnO/Au hybrid catalytic performance in detail. To further investigate the influence of Au NPs on the photocatalytic activity of ZnO/Au hybrid, a series of control experiments were carried out. Firstly, Au colloids with different Au NPs size (5, 10, 20, 30, 50 nm) were synthesized, and then ZnO NRs on ITO were immersed into the Au colloid for about 30 min. Then the photocatalytic capability of ZnO/Au NRs with different Au NPs sizes was investigated on degradation of MB (see Fig. 9). It shows that the photocatalytic activity for degradation of MB increases with the decreasing of Au NPs size. And the highest photocatalytic activity

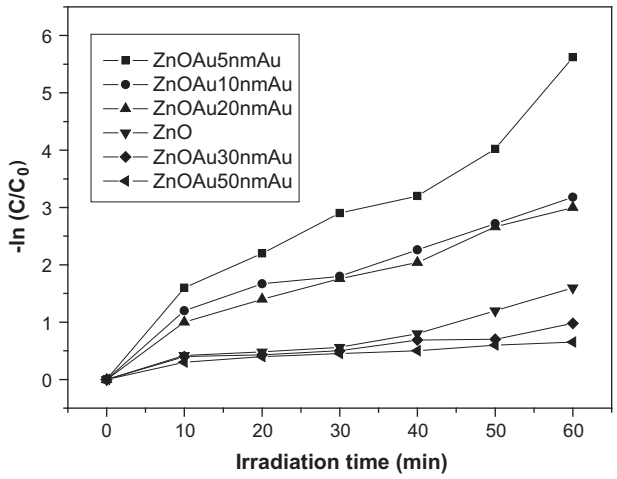

Fig. 9. Photocatalytic activities of ZnO/Au Hybrids upon irradiation time with different Au NPs sizes.

for degradation of MB can be achieved with the size of 10 nm. The enhancement of the photocatalytic activity is achieved when the adsorbed size of Au NPs is smaller than 20 nm. Similar conclusion has been reported by Wu et al., who have also found that the photocatalytic activities of ZnO NRs are affected by the size of the Au NPs [29]. In their work, it also was found that the enhancement is more pronounced as the size of the Au NPs is decreased. They thought that in the case of the Au nanoparticles with larger sizes, Schottky barriers would exist at the junction of the Au–ZnO nanorods just like they are in bulk phases. In addition, the intensity of the incident irradiation for ZnO nanorod absorption will be reduced by scattering due to the larger Au NPs on the tips. The dramatic decrease in the apparent photocatalytic activity of the ZnO/Au hybrids with larger Au NPs size (30 nm, 50 nm) in comparison with that of the ZnO NRs is suggested to be ascribed to the lower concentrations of the photogenerated electron–hole pairs in ZnO/Au hybrids.

To investigate the effect of initial concentration of MB on the photocatalytic degradation rate, MB with various concentrations ranging from 3×10^{-5} to 9×10^{-5} M was used, and the experimental results were shown in Fig. 10. The photodegradation rate constant was calculated according to $\ln(C/C_0) = kt$, which was mentioned earlier. It is revealed that the reaction rate constants decreased with increasing of initial MB concentration. The result

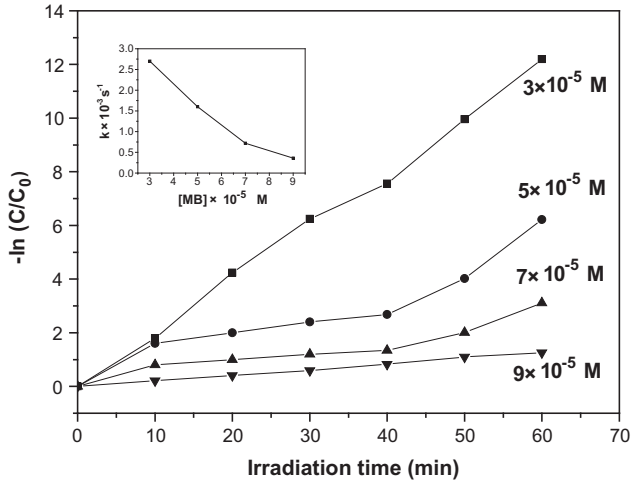

Fig. 10. Plot of variation of concentration of MB (■) 3×10^{-5}, (●) 5×10^{-5} M, (▲) 7×10^{-5} M, and (▼) 9×10^{-5} M upon irradiation time in the presence of Sample A. Inset shows plot of photodegradation rate constant for various concentration of MB.

is in accordance with the fact that when the initial concentration of MB increases, MB adsorbs the light except the ZnO/Au NRs [30]. In addition, it may reach saturation in the adsorption of MB on the surface of ZnO/Au NRs.

4. Conclusions

In summary, we have presented a simple method to prepare ZnO/Au composite nanoarrays, which showed better photocatalytic efficiency than pure ZnO when proper Au NPs were loading. SEM, EDS, and UV–visible spectroscopy confirmed the formation of ZnO/Au NRs. The improved photocatalytic efficiency is ascribed to Au loading, which decreased the recombination of electrons and holes. The density and size of Au NPs on the ZnO NRs can be easily controlled by altering the concentration of $HAuCl_4$. The photocatalytic efficiency is affected by the density of Au NPs on the surface of ZnO NRs, in which ZnO/Au NRs with optimal density (9 per NR) display the highest photocatalytic efficiency. It is believed that as-synthesized ZnO/Au NRs are stable and efficient for the environmental purification of organic pollutants in aqueous solution. In addition, this approach used no other organic surfactant for growing Au NPs, so that it is environmental friendly and convenient.

Acknowledgment

This work was supported by the China Postdoctoral Science Foundation No. 20100481068.

References

[1] A. Mills, S.L. Hunte, J. Photochem. Photobiol., A 108 (1997) 1–35.
[2] S. Anandan, M. Yoon, J. Photochem. Photobiol., C 4 (2003) 5–18.
[3] E. Szabo-Bardos, H. Czili, A. Horvath, J. Photochem. Photobiol., A 154 (2003) 195–201.
[4] V. Subramanian, E.E. Wolf, P.V. Kamat, J. Phys. Chem. B 107 (2003) 7479–7485.
[5] Y. Tian, T. Tatsuma, J. Am. Chem. Soc. 127 (2005) 7632–7763.
[6] R. Costi, A.E. Saunders, E. Elmalem, A. Salant, U. Banin, Nano Lett. 8 (2008) 637–641.
[7] M. Jakob, H. Levanon, P.V. Kamat, Nano Lett. 3 (2003) 353–358.
[8] H.B. Zeng, P.S. Liu, W.P. Cai, S.K. Yang, X.X. Xu, J. Phys. Chem. C 112 (2008) 19620–19624.
[9] T. Mokari, C.G. Sztrum, A. Salant, E. Rabani, U. Banin, Nat. Mater. 4 (2005) 855–863.
[10] T. Mokari, E. Rothenberg, I. Popov, R. Costi, U. Banin, Science 304 (2004) 1787–1790.
[11] J.S. Lee, E.V. Shevchenko, D.V. Talapin, J. Am. Chem. Soc. 130 (2008) 9673–9675.
[12] H. Yu, M. Chen, P.M. Rice, S.X. Wang, R.L. White, S.H. Sun, Nano Lett. 5 (2005) 379–382.
[13] T. Mokari, A. Aharoni, I. Popov, U. Banin, Angew. Chem., Int. Ed. 45 (2006) 8001–8005.
[14] A.M. Schwartzberg, D.C. Grant, A. Wolcott, C.E. Talley, T.R. Huser, R. Bogomolni, J.Z. Zhang, J. Phys. Chem. B 108 (2004) 19191–19197.
[15] Y.C. Liu, M.Y. Zhong, G.Y. Shan, Y.J. Li, B.Q. Huang, G.L. Yang, J. Phys. Chem. B 112 (2008) 6484–6489.
[16] R.K. Joshi, Q. Hu, F. Alvi, N. Joshi, A. Kumar, J. Phys. Chem. C 113 (2009) 16199–16202.
[17] Y.J. Lee, D.S. Ruby, D.W. Peters, B.B. Mckenzie, J.W.P. Hsu, Nano Lett. 8 (2008) 1501–1505.
[18] P.H. Kasai, Phys. Rev. 130 (1963) 989–995.
[19] H.J. Egelhaaf, D. Oelkrug, J. Cryst. Growth 161 (1996) 190–194.
[20] L. Jing, Y. Qu, B. Wang, S. Li, B. Jiang, L. Yang, W. Fu, H. Fu, J. Sun, Sol. Energy Mater. Sol. Cells 90 (2006) 1773–1787.
[21] L.M. Chen, L.B. Luo, Z.H. Chen, M.L. Zhang, A.J. Zapien, C.S. Lee, S.T. Lee, J. Phys. Chem. C 114 (2010) 93–100.
[22] K. Vanheusden, W.L. Warren, C.H. Seager, D.R. Tallant, J.A. Voigt, B.E. Gnade, J. Appl. Phys. 79 (1996) 7983–7990.
[23] H.F. Lin, S.C. Liao, S.W. Hung, J. Photochem. Photobiol., A 174 (2005) 82–87.
[24] H. Goto, Y. Hanada, T. Ohno, M. Matsumura, J. Catal. 225 (2004) 223–229.
[25] J.S. Curran, D. Lamouche, J. Phys. Chem. 87 (1983) 5405–5411.
[26] A. Wood, M. Giersig, P. Mulvaney, J. Phys. Chem. B 105 (2001) 8810–8815.
[27] V. Subramanian, E.E. Wolf, P.V. Kamat, J. Am. Chem. Soc. 126 (2004) 4943–4950.
[28] Y. Lin, Y. Hsu, S. Chen, Y. Lin, L. Chen, K. Chen, Angew. Chem., Int. Ed. 48 (2009) 7586–7590.
[29] J.J. Wu, C.H. Tseng, Appl. Catal., B 66 (2006) 51–57.
[30] N. Sobana, M. Swaminathan, Sol. Energy Mater. Sol. Cells 91 (2007) 727–734.